PCCP

A New Way of Studying Chemical Reactions: A Hand-in-Hand URVA and QTAIM Approach

Journal:	*Physical Chemistry Chemical Physics*
Manuscript ID	CP-ART-04-2019-001933.R1
Article Type:	Paper
Date Submitted by the Author:	14-Jun-2019
Complete List of Authors:	Nanayakkara, Sadisha; Southern Methodist University, Chemistry Kraka, Elfi; Southern Methodist University, Chemistry

SCHOLARONE™
Manuscripts

Journal Name

ARTICLE TYPE

Cite this: DOI: 10.1039/xxxxxxxxxx

A New Way of Studying Chemical Reactions: A Hand-in-Hand URVA and QTAIM Approach†

Sadisha Nanayakkara[a] and Elfi Kraka*[b,c]

Received Date
Accepted Date

DOI: 10.1039/xxxxxxxxxx

www.rsc.org/journalname

Bond formation and bond cleavage processes are central to a chemical reaction. They can be investigated by monitoring changes in the potential energy surface (PES) or changes in the electron density (ED) distribution $\rho(\mathbf{r})$ taking place during the reaction. However, it is not yet clear how the corresponding changes in the PES and ED are related, although the connection between energy and density has been postulated in the famous Hohenberg-Kohn theorem. Our Unified Reaction Valley Approach (URVA) identifies the locations of bond formation/cleavage events along the reaction path via the reaction path curvature peaks and their decomposition into the internal coordinate components associated with the bond to be formed or cleaved. One can also investigate bond formation/cleavage events using the Quantum Theory of Atoms-in-Molecule (QTAIM) analysis by monitoring changes in the topological properties of $\rho(\mathbf{r})$ and the associated Laplacian $\nabla^2\rho(\mathbf{r})$. By a systematic comparison of these two approaches for a series of ten representative chemical reactions ranging from hydrogen migration, cycloaddition reactions to gold(I) catalysis, we could for the first time unravel the PES-ED relationship. In the case of a bond formation, all changes in the ED occur shortly before or at the corresponding curvature peak, and in a bond cleavage the ED changes occur at or shortly after the curvature peak. In any case the ED changes always occurred in the vicinity of the curvature peak in accordance with the Hohenberg-Kohn theorem. Our findings provide a comprehensive view on bond formation/cleavage processes seen through the eyes of both the PES and ED and offer valuable guidelines where to search for significant ED changes associated with a bond formation or cleavage events.

1 Introduction

Bond formation and bond cleavage are central to a chemical reaction and this provokes one to pinpoint these chemically invaluable events along a reaction path connecting reactants and products. The general approach would be to follow this reaction path and quantitatively account for the bonding status of the reaction complex (i.e. the union of reacting molecules) on the grounds of monitoring some property that is sensitive to bond formation/cleavage events. There have been a number of studies along these lines using as reaction path the intrinsic reaction coordinate (IRC) of Fukui.[1] Based on the choice of bond-sensitive property, these approaches can be classified into two main categories: those which employ features of the potential energy surface (PES), i.e. energy related properties and those which use topological properties of the electron density (ED) as summarized in Figure 1.

With regard to features of the PES, Komorowski and coworkers[2] introduced a novel perspective to study bond formation/cleavage using so-called atomic fragility parameter $a_\xi{}^A$, that is based on the trace of the Hessian matrix. Evaluation of $a_\xi{}^A$ along IRC generates a spectra-like profile termed reaction fragility spectrum where regions of $a_\xi{}^A$ with $a_\xi{}^A < 0$ correspond to bond dissociation and $a_\xi{}^A > 0$ to bond formation. Toro-Labbé et al. characterized the reaction mechanism of 1,3-intramolecular hydrogen transfer reactions by identifying different regions along the IRC, utilizing energy and reaction force profiles as the operating tools;[3] a recurring approach in several mechanistic studies.[4,5]

We use the *Unified Reaction Valley Approach* (URVA) developed by Kraka and Cremer[6–8] which is based on the reaction path Hamiltonian of Miller, Handy and Adams.[9] URVA utilizes the scalar curvature $\kappa(s)$[10] of the reaction path to identify bond formation/cleavage as a reaction proceeds. The curvature maxima

[a] *Computational and Theoretical Chemistry Group (CATCO), Department of Chemistry, Southern Methodist University, 3215 Daniel Avenue, Dallas, Texas 75275-0314, United States.*

[b] *Computational and Theoretical Chemistry Group (CATCO), Department of Chemistry, Southern Methodist University, 3215 Daniel Avenue, Dallas, Texas 75275-0314, United States. E-mail: ekraka@smu.edu*

[c] *In memoriam of Dieter Cremer*

† Electronic Supplementary Information (ESI) available: Supplementary data associated with this article can be found, in the online version. Cartesian coordinates of the stationary points and reaction movies of the reactions **R1** - **R10** are included. See DOI: 10.1039/xxxxxxxxxx/

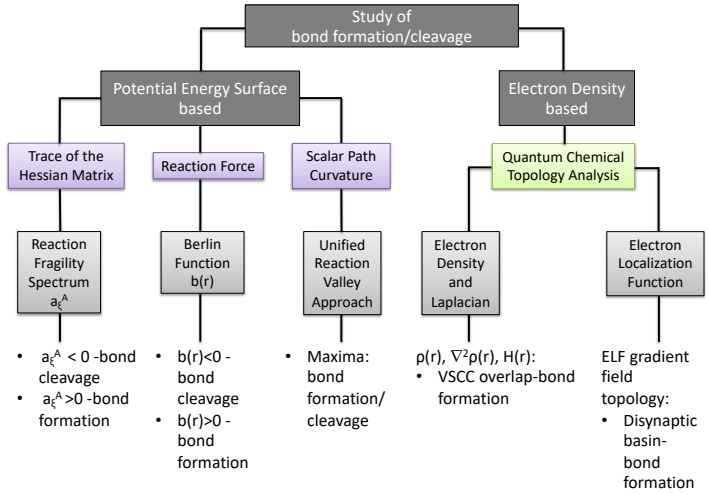

Fig. 1 Classification and summary of the main features regarding bond formation/cleavage for some reaction path based methods.

Kn indicate locations on the reaction path where the reaction coordinate drastically steers from a subset of degrees of freedom to another subset, suggesting a chemical event (conformational, rehybridization, bond formation, bond cleavage, etc.) (See Section 2 for a detailed description of URVA.) URVA has been successfully applied in our research to organic reactions,[11–15] homogenous catalysis[16,17] as well as chemical reactions taking place in an enzyme.[18]

Complementary to the quantum chemical study of PES related properties, a description of bond cleavage/formation processes can also be based on the physical observable, ED, $\rho(\mathbf{r})$. Hohenberg and Kohn[19] showed that the energy of a non-degenerate electronic ground state of a molecule is a unique functional of the ED implying that other chemical and physical properties can also be related to the ED. Thus the analysis of ED redistributions along the reaction path provides a rational approach to study bond formation and cleavage in concert with the changes of the PES related properties, which is the underlying motivation throughout our work. The pioneering work of Bader's Quantum Theory of Atoms-in-Molecules (QTAIM) analysis exploits the assertions in Hohenberg-Kohn theorem (HKT) by providing a rigorous protocol to define chemical bonding in terms of topological properties of the ED.[20–26] Another appealing method based on the ED is the electron localization function approach of Becke and Edgecombe.[27] This was further developed by Silvi and Krokidis[28] in their bonding evolution theory methodology for the quantitative study of chemical bonding along the reaction path. A substantial amount of work has been done within these frameworks to provide a wealth of information about reaction mechanisms, essentially for identifying the bond formation/cleavage processes, as highlighted in the recent works by Abjieufack et al.[29] on 1,3-dipolar cycloaddition reaction mechanism and also in Zahedi and co-workers'[30] coupled analysis using bonding evolution theory and noncovalent interaction index. In the work of Zalazar and co-workers'[31] aimed at the study of bond formation/cleavage events in zeolite-catalyzed reactions, various topological properties along the IRC were used as direct indicators to disclose the bonding status of selected bonds.

Despite these numerous studies, there is still a missing link bridging the features of the PES with those of the ED to provide a deeper insight into bond formation/cleavage events. In this respect, it is worth mentioning the work of Chakraborty et al.[32] where they introduced a chemical binding indicator $b(r)$, combining the Berlin function[33] and the derivative of the ED. The regions of space where $b(r) < 0$ indicate a bond cleavage event, and $b(r) > 0$ indicate a bond formation event. Another study spanning both PES and ED scopes is that of Sun and co-workers'[34] involving the conventional energy scheme of stationary points and intermediates, and more interestingly the topological analysis of the ED along the reaction path emphasizing on bond formation/cleavage structures. By monitoring gradient paths of the ED, they located the points on the reaction path where gradient paths appear/disappear, signifying formation/cleavage of respective bonds and as well as points corresponding to maximum of the Laplacian $\nabla^2\rho(\mathbf{r})$ which they termed as a *structure transition state*.

The preceding studies describing bond formation/cleavage along the reaction path based on the features of the PES, ED or a composite of both, provoked us to systematically explore how the changes in the PES and ED pertinent to bond formation/cleavage processes are related along the reaction path. Simply put, are the significant changes in the features of the PES and ED, that govern the formation or a rupture of a bond, analogous? If we monitor formation/cleavage of a chemical bond along the reaction path, can we identify if the PES and ED changes occur simultaneously or concomitantly? If these changes occur at different points along the reaction path, what is the order of appearance? One final question to pose is, how to use this new-found relation between features of the PES and ED to investigate bond formation/cleavage events along the reaction path in the most efficient way?

To answer these questions, we performed a comprehensive study linking features of the PES and ED for a series of chemical reactions covering a wide range of different bond formation/cleavage mechanisms, including hydrogen migration reactions, pericyclic reactions such as the Diels-Alder reaction, and non-catalyzed/catalyzed sigmatropic rearrangement reactions. While we employed the URVA toolbox for investigating PES features, we used the QTAIM methodology for analyzing ED redistributions along the reaction path. Whereas the curvature maxima explicitly reveal the bond formation/cleavage processes along the reaction path, it is a more challenging task identifying the specific changes in the ED that could be closely associated with formation/cleavage of a bond. Bader's analysis based on topological properties of the ED at bond critical points (bcp) c, $\rho(c)$, provides a rational basis to identify formation or a cleavage of a bond. The appearance of a bond path indicates the formation of a new bond and conversely, the disappearance of a bond path is associated with a cleavage of an existing bond. However, an ED measure solely based on the bond path could be misleading and has to be complemented with other topological properties. While the

This journal is © The Royal Society of Chemistry [year]

gradient vector field $\nabla\rho(\mathbf{r})$, can be used to further characterize the bond paths to some extent, more information of chemical interest can be extracted from the Laplacian $\nabla^2\rho(\mathbf{r})$ as it displays the regions of local concentration and depletion of charge. Additionally, as pointed out by Bader and co-workers, the $\nabla^2\rho(\mathbf{r})$, yields a density shell structure corresponding to the quantum shell structure.[35,36] Thus the outermost region of charge concentration ($-\nabla^2\rho(\mathbf{r})$) represents the valence shell, termed as valence shell charge concentration (VSCC). The VSCC has been employed in several works to study bond formation/cleavage events.[37,38] For a bonded atom pair, the covalent character increases with approaching VSCC and, vice versa. Therefore we also used the VSCC overlap begin/end points as flag points to monitor bond formation/cleavage processes. For the characterization of the covalent nature of a chemical bond, the Cremer and Kraka criterion[39] draws a sufficient condition based on the total electronic energy density $H(c)$ at bond critical point c, which states that $H(c) < 0$ is indicative of a covalent interaction whereas $H(c) > 0$ is indicative of an electrostatic interaction. Thus we monitored changes in the bond critical points, bond paths, $H(c)$, $\nabla^2\rho(c)$ and VSCC in order to identify bond formation/cleavage events, which we defined as E points. These E points include (a) catastrophe points attributed to the ED topology: appearance/disappearance of a bond path, coalescence of bond and ring critical points, and (b) the initial point of partial overlap between the VSCCs of the two atoms of interest and conversely, the terminating point of this partial overlap separating the VSCCs to respective atomic basins.

The objectives of this study were the following: (i) To elucidate and comment on bond formation/cleavage processes along the reaction path with the combined use of URVA and QTAIM; (ii) To probe the topology of the Laplacian at curvature peak positions; (iii) To understand the relationship between maxima in the URVA curvature and E points, moreover to compare their relative locations along the reaction path; (iv) To evaluate QTAIM properties at the bond critical points, at the stationary points, e.g. reactants, products, transition state, at the reaction path curvature maxima, curvature minima and selected E points.

2 Computational Methods

The theoretical basis underlying URVA has been thoroughly described in several publications[14,15,40–43] as well as in some review articles.[6–8,44] Therefore, we will provide only a brief overview of the major features of URVA, focusing on those used in this work. URVA follows the movement of the reaction complex (RC, the union of reacting molecules) along the reaction path on the PES from reactants to products via the transition state spanning the entire reaction path region from entrance to exit channel. As a chemical reaction proceeds, the undergoing electronic structure changes of the RC are registered by its vibrational modes. The change in the vibrations results in a change of their coupling with the translational motion along the reaction path which can be monitored by the so-called curvature coupling coefficients $B_{\mu,s}$[8–10] at each path point s. Large electronic structure changes, i.e. the formation/cleavage of a chemical bond results in large $B_{\mu,s}$ values. The $B_{\mu,s}$ coefficients define the scalar reaction path curvature $\kappa(s)$[8–10] which measures the curving of the reaction path. Thus, analysis of $\kappa(s)$ along the reaction path in the form of a curvature profile provides a direct connection to identify the electronic structure changes of the RC during the reaction. The curvature profile is an ensemble of curvature maxima Kn and minima Mn. The Kn points indicate important chemical events (e.g. bond formation/cleavage, rehybridization, or charge transfer and polarization, etc.) while at the Mn locations bordering a peak, the RC falls to a neutral state or one with lower activity. The Mn can be associated with *hidden intermediates*[6,7] which means a conversion to a real intermediate under specific reaction conditions is possible, e.g. by adding a catalyst.[12,14–17] We coined the region stretching from one curvature minimum to the next enveloping a curvature maximum a *reaction phase*.[6,7] In this way each curvature profile is composed of a series of reaction phases, which can be used as the fingerprint of the reaction. A key feature of URVA related to our current work is the decomposition of the curvature into curvature components[10] unravelling which internal coordinates (bond length, bond angle, dihedral angle, etc.) contribute to a certain curvature peak. A curvature component can be supportive (positive $\kappa(s)$ values) or resisting (negative $\kappa(s)$ values) to the chemical event its describing. In this way the locations of bond formation/cleavage events can be uniquely identified.

We included in our current study the ten reactions **R1** - **R10** shown in Figure 2 previously investigated with URVA.[6,10–12,16,17,45] The reactions were chosen to cover a wide range of different bond formation/cleavage scenarios. We focused in particular on the bond length curvature components and their associated curvature peaks describing bond formation/cleavage events. For each of the reactions **R1** - **R10** the same model chemistry was used as in the previous URVA study: UMP2[46,47]/6-31G(d,p)[48] for **R1** and **R2**, MP2/6-31G(d,p) for **R3** and **R4**, B3LYP/Def2-SVP[49]/ECP(Au)[50] for **R5**, B3LYP[51]/6-31G(d,p) for **R6** and **R8**, B3LYP/6-311+G(d,p)[52] for **R7**, B3LYP/6-31+G(d,p)[53] for **R9** and B3LYP/6-31+G(d,p)/SDD[54] for **R10**. A sufficiently large range of points around each curvature peak was analyzed to identify all important E points includ-

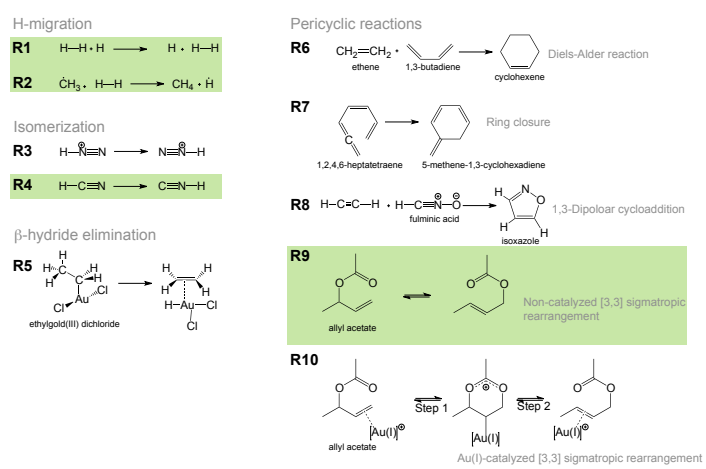

Fig. 2 Reactions **R1-R10** investigated in this work. Reactions **R1, R2, R4** and **R9** indicated by green boxes are discussed in detail in the manuscript. The remaining reactions are discussed in Electronic Supplementary Information (ESI).

ing the VSCC overlap begin/end points. The ED at these points was analyzed to determine the corresponding $\rho(c)$, $\nabla^2\rho(c)$, ε and $H(c)$ values. Apart from curvature peaks, we also investigated the ED at other points of interest along the reaction pathway with the QTAIM methodology, i.e. at the location of reactants (R), products (P) and transition states (TS), as well as at the Mn. All quantum chemical calculations were carried out with the GAUSSIAN16 program package,[55] the ED analysis was performed with the program the AIMALL[56] and URVA with the program package COLOGNE2019.[57]

3 Results and Discussion

The results of this work are presented for 4 selected reactions (see Figure 2), each of the subsections dedicated to one of the reactions **R1**, **R2**, **R4** and **R9**. The rest of the reactions are discussed in electronic supplementary information (ESI). The QTAIM parameters evaluated at curvature peak and E points of importance for the bond formation/cleavage processes and at the stationary points R, TS, P are tabulated in Tables 1-4. In Figures 3-6 the scalar curvature $\kappa(s)$ and its decomposition into bond length contributions relevant for the bond formation/cleavage processes are shown as a function of the reaction parameter s as well as $\nabla^2\rho(\mathbf{r})$ contour plots with bond paths and bond critical points at Kn, Mn, E points and stationary points listed in Tables 1-4. In addition, Cartesian coordinates of all stationary points and reaction movies of the reactions **R1** - **R10** are included in ESI.

3.1. R1: H + H_2 reaction This elementary reaction has been often used as a prototype for studying bimolecular reactions in many theoretical and experimental aspects.[58] We used this reaction as a starting point for our combined URVA and QTAIM analysis to deduce the link between the relative locations of the significant E and curvature points on the reaction path reflecting HH breakage and HH bond formation. Because of symmetry, both forward and reverse reactions are identical. As shown in Figure 3-A the curvature profile features two peaks, one closely before the TS at s = -0.20 units and one at s = +0.20 units being related to the equivalent reverse reaction. The first peak is dominated by the bond formation component H2H3 (numbering the RC as H1-H2$\cdots$ H3) which is supportive (positive sign) whereas the bond cleavage component H1H2 is negative indicative of resistance to bond breaking. At the TS, with equal H1-H2 and H3-H3 distances and a 3 electron-3 center (3e-3c) bonding situation, a curvature minimum is located, denoting the starting point of the reversion of the role of the H1H2 and H2H3 components. Cleary, bond formation proceeds bond breakage leading to a non-classical 3e-3c bonding situation between s = -0.20 and +0.20 units.

The ED starts to accumulate in the region between H2 and H3 at E (-0.30 s units, see Table 1) initiating the VSCC overlap which

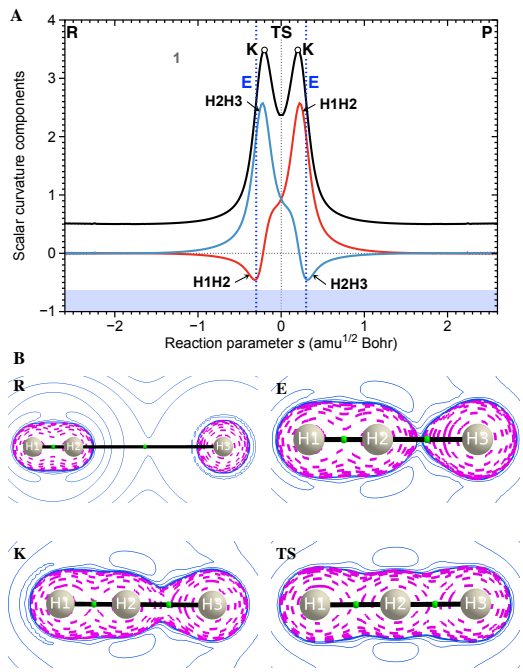

Fig. 3 R1 A) Scalar curvature (shifted by 0.5 s units for comparison with components) as a function of the reaction parameter s (solid black line). The decomposition of scalar curvature into components is given in color. The borders of the reaction phases are indicated by vertical dashed lines at curvature points M1,M2,M3,etc. The TS at s = 0 amu$^{1/2}$ Bohr is also indicated by a vertical dashed line. R and P mark the first and last curvature points, corresponding to reactant and product respectively. K denotes a curvature peak. E denotes a special point in electron density shown by a blue vertical dashed line. Values in grey 1,2,3,etc. indicate reaction phases. B) Laplacian contour plots of selected curvature points R,E,K,TS, plotted in the molecular plane. The dashed (pink) contours denote regions of charge concentration where $\nabla^2\rho(\mathbf{r}) < 0$, and the solid (blue) contours denote regions of charge depletion where $\nabla^2\rho(\mathbf{r}) > 0$.

Table 1 Local topological properties of the electron density $\rho(c)$ calculated at the bond critical points c along the IRC for the forming bond H3H2 and cleaving bond H1H2, values in bold are for curvature peak data. s reaction parameter, $\rho(c)$ electron density, $\nabla^2\rho(c)$ Laplacian, $H(c)$ total energy density, ε ellipticity calculated at the UMP2/6-31G(d,p) level of theory

Numbering	Bond	Character	s (amu$^{1/2}$Bohr)	$\rho(c)$ (e/Bohr^3)	$\nabla^2\rho(c)$ (e/Bohr^5)	ε ($\times 10^{-15}$)	$H(c)$ (Hartree/Bohr^3)
	H2H3	R	-2.6799	0.0031	0.0086	0.0000	0.0004
H1—H2 + H3		E	-0.2999	0.0820	-0.0110	0.4441	-0.0335
		K	-0.2000	0.1010	-0.0654	0.2220	-0.0490
		TS	0.0000	0.1557	-0.3345	1.1102	-0.1128
	H1H2	R	-2.6799	0.2752	-1.4181	0.0000	-0.3610
		E	-0.2999	0.2400	-1.0262	0.2220	-0.2729
		K	-0.2000	0.2183	-0.8177	0.2220	-0.2244
		TS	0.0000	0.1557	-0.3345	1.3323	-0.1128

This journal is © The Royal Society of Chemistry [year]

is also reflected by the Laplacian revealing that the ED of the incoming H atom is polarized towards the ED distribution of H_2. This E point occurs fairly close to the curvature peak K, which signifies the formation of the new bond. It is interesting to note that after the E point, the supportive dominance of H2H3 declines whereas the resistance of H1H2 bond breakage turns into support and the 3e-3c bond starts to get established, showing that for this simple reaction PES and ED features are synchronized.

3.2. R2: CH_3+H_2 reaction In this hydrogenation reaction of CH_3 radical,[6,14,40] we can recognize two distinct curvature peaks, K1 at -0.08 s units and K2 at +0.60 s units (see Figure 4-A). The first curvature peak K1 is dominated by the H2H6 bond component supporting bond breaking. In a previous URVA study[40], using electron difference density distribution maps $\Delta\rho(\mathbf{r})$, it has been shown that when CH_3 and H_2 approach each other the HH bond becomes polarized towards the negatively charged C atom which in turn leads to a draining of the ED from the HH bond region. Examining the $\nabla^2\rho(c)$ topology at the initial VSCC overlap point E1 (-0.16 s units, see Figure 4-B) confirmed this observation, where it was seen that the ED distribution in the region between H2 and H6 is slightly perturbed and after this point starts to accumulate between the C1 and H2 atomic basins. This is also reflected by $H(c)$ and $\nabla^2\rho(c)$ of C1H2 (see Table 2) which have become negative at this point. As seen from the curvature component C1H2 (see Figure 4-A), the resisting contribution which is at a maximum at E1, starts to recede gradually after E1 and converts into a supporting one at the TS which is shortly after K1 peak. In this way the ED flow from the H2H6 bond region to the C1H2 region causes the latter to become less resisting to bond formation. Meanwhile, the negative $H(c)$ and $\nabla^2\rho(c)$ values for H2H6 (see Table 2) are becoming more positive along the reaction path through the K1 peak implying the loss of covalent character. The other peak K2 at +0.60 s units is resulting from finalization of the C1H2 bond formation as reflected in its supporting contribution to the peak. Here, there is no charge concentration between H2H6 atomic basins as exhibited by the Laplacian topology (see Figure 4-B) and positive $\nabla^2\rho(c)$ value (=0.03, see Table 2). In contrast, C1H2 has negative $\nabla^2\rho(c)$ and $H(c)$ values, evidence of well-established covalent nature of the C1H2 bond. The charge concentration around H6 atom starts adapting its spherical character at E2 (+0.42 s units, see Figure 4-B), when the ED starts to recede between the H2H6 region indicating the detachment of VSCC overlap. With regard to the H2H6 component, E2 resides in a plateau of the H2H6 curvature component (in green, see Figure 4-A) after which supporting contribution of H2H6 rapidly declines and turn into a resisting one along the path. This reveals that when the ED starts to reorganize into the CH bond situation of CH_4 and the ED distribution around H6 becomes spherical,

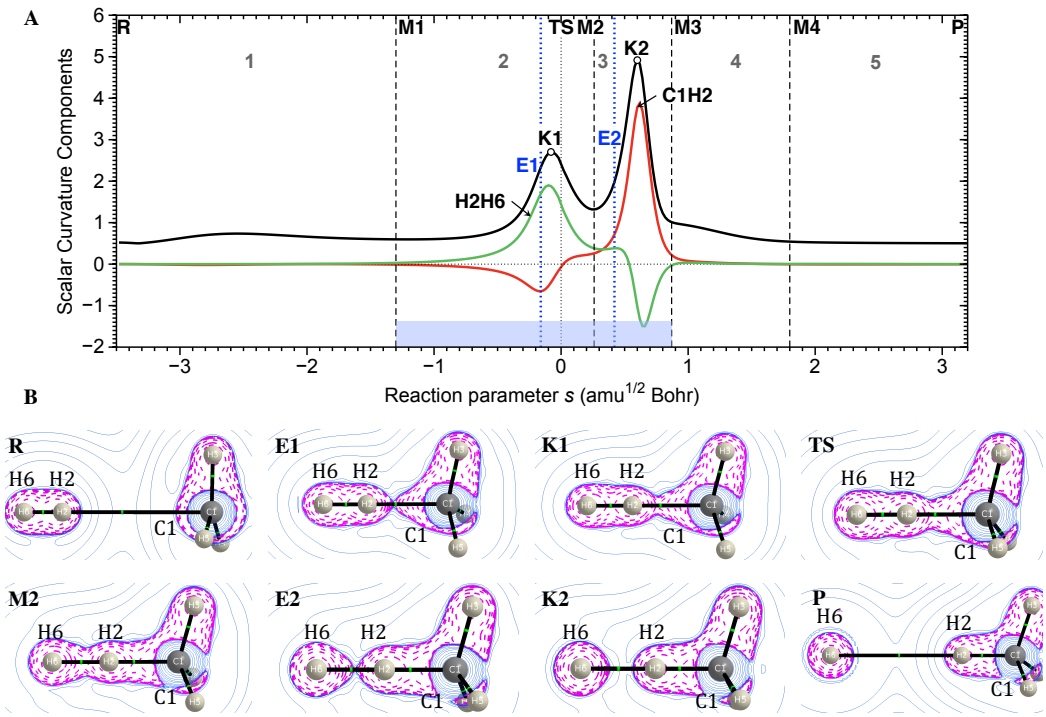

Fig. 4 R2 A) Scalar curvature (shifted by 0.5 s units for comparison with components) as a function of the reaction parameter s (solid black line). The decomposition of scalar curvature into components is given in color. The borders of the reaction phases are indicated by vertical dashed lines at curvature points M1,M2,M3,etc. The TS at s = 0 amu$^{1/2}$ Bohr is also indicated by a vertical dashed line. R and P mark the first and last curvature points, corresponding to reactant and product respectively. K1,K2,etc. denote curvature peaks. E1,E2,etc. denote special points in electron density shown by blue vertical dashed lines. Values in grey 1,2,3,etc. indicate reaction phases and highlighted region in blue shows the chemical phases. B) Laplacian contour plots of selected curvature points R,E1,K1,TS,E2,K2,P, plotted in the H2-C1-H3 plane. The dashed (pink) contours denote regions of charge concentration where $\nabla^2\rho(\mathbf{r}) < 0$, and the solid (blue) contours denote regions of charge depletion where $\nabla^2\rho(\mathbf{r}) > 0$.

Table 2 Local topological properties of the electron density $\rho(c)$ along the IRC calculated at the bond critical points c for the forming bonds C1H2 and cleaving bond H2H6, values in bold are for curvature peak data. s reaction parameter, $\rho(c)$ electron density, $\nabla^2\rho(c)$ Laplacian, $H(c)$ total energy density, ε ellipticity calculated at the UMP2/6-31G(d,p) level of theory

Numbering	Bond	Character	s (amu$^{1/2}$Bohr)	$\rho(c)$ (e/Bohr^3)	$\nabla^2\rho(c)$ (e/Bohr^5)	ε ($\times 10^{-9}$)	$H(c)$ (Hartree/Bohr^3)
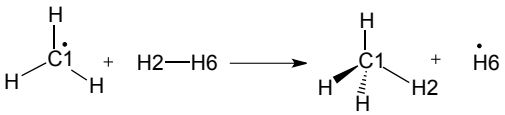	C1H2	R	-3.4799	0.0056	0.0152	0.4728	0.0005
		M1	-1.2999	0.0303	0.0635	0.3733	-0.0033
		E1	-0.1599	0.0971	-0.0067	0.6894	-0.0444
		K1	**-0.0799**	**0.1090**	**-0.0461**	**0.7083**	**-0.0551**
		TS	0.0000	0.1234	-0.1020	0.3122	-0.0690
		M2	0.2599	0.1824	-0.3726	1.6970	-0.1354
		E2	0.4199	0.2229	-0.5904	1.0904	-0.1938
		K2	**0.5998**	**0.2651**	**-0.8636**	**0.4860**	**-0.2704**
		M3	0.8598	0.2821	-0.9934	0.0416	-0.3055
		M4	1.7998	0.2834	-1.0123	1.4754	-0.3078
		P	3.1998	0.2807	-0.9943	1.3972	-0.3022
	H2H6	R	-3.4799	0.2748	-1.4133	0.0001	-0.3599
		M1	-1.2999	0.2714	-1.3639	0.0022	-0.3498
		E1	-0.1599	0.2153	-0.7853	0.0345	-0.2180
		K1	**-0.0799**	**0.1988**	**-0.6424**	**0.0023**	**-0.1847**
		TS	0.0000	0.1783	-0.4839	0.0485	-0.1477
		M2	0.2599	0.1120	-0.1068	0.0052	-0.0591
		E2	0.4199	0.0826	-0.0100	0.1444	-0.0339
		K2	**0.5998**	**0.0592**	**0.0340**	**0.0615**	**-0.0189**
		M3	0.8598	0.0411	0.0468	0.1433	-0.0098
		M4	1.7998	0.0140	0.0355	0.2960	0.0001
		P	3.1998	0.0033	0.0090	0.0666	0.0005

the H2H6 bond cleavage process has reached completion and the corresponding curvature component adjust accordingly. In other words, when the ED stops flowing into the H2H6 interatomic region, the H2H6 curvature component does no longer affect the curving of the reaction path. Compared with the H + H_2 reaction, the first half of the CH_3+H_2 reaction exhibits a similar curvature pattern with the inclusion of an E point, but the role of the HH component is reversed. The former has a resisting contribution to the first curvature peak from the HH bond component to be broken while latter shows a supporting contribution (diminishing after E1) which can be explained by the enhanced polarization in the presence of CH_3 radical.[14] The E1 point associated with the CH bond formation precedes the K2 peak and is located in the vicinity of the K1 peak. On the other hand, the E2 point associated with the HH bond cleavage follows after K1 peak and it is located near K2 peak. The ED changes before a peak add up to the bond formation and the reorganizations after a peak signaled completion of bond cleavage, herein providing further insight into the link between PES and ED features.

***3.3. R4: Isomerization* of HCN** This simple gas phase reaction of hydrogen cyanide rearranging to hydrogen isocyanide has been extensively studied using several theoretical tools[3,59–61] including URVA method.[10] Here, we intended to revisit this reaction with our combined analogy, thereby facilitating better understanding of its bond formation/cleavage processes along the IRC. Also, this reaction can be seen in connection with HN_2^+ reaction as characterized by similar curvature shape. In the curvature profile, the only curvature peak K1 at +0.76 s units decomposes into major supporting contributions from C1H3 and N2H3 bonds. At this peak point, a bond path is found for N2H3 having a negative $H(c)$. It was formerly proposed that this reaction proceeds via a cyclic, non-classical structure (partial 2e-3c bonding) located after the TS.[10] However, the ED analysis revealed the presence of a bond switching structure where the C1H3 bond path disappears and N2H3 bond path appears at +0.02 s units (at E1, see Figure 5-B). This is rather close to the TS in which the N2H3 bond path is still absent. Since at E1 the bond path has been already switched from C to N atom, E1 is in fact a stable structure according to structural stability requirements.[22,36] An infinitesimal shift in the direction of the TS will result in a bond catastrophe point where the H atom will be directly linked to the CN bcp yielding a catastrophe point of the conflict type.[22,36] (For our discussion investigating E1 is sufficient, which is close to the catastrophe point.) At E1 for N2H3, $H(c)$ is negative suggesting a covalent interaction and ε is significantly high (=0.92, see Table 3) resulting from the distorted T-shaped ED distribution at that point. The negative $H(c)$ progressively increases where at +0.76 s units it marks the finalization of the N2H3 formation as evident by the corresponding curvature peak K1 (see Figure 5-A). Also, an interesting observation about the topology of Laplacian charge density at K1 is that it starts depleting between the C1H3 atomic basins at this point, eventually rearranging to more or less spherical form around C1 and H3 atoms. By the comparison of contour plots of $\nabla^2\rho(c)$ for M1 and its counterpart M2 (see Figure 5-B), this topological change is more distinct. In comparison to the analogous HN_2^+ system, it can be inferred that changing from symmetric HN_2^+ system to one that is asymmetric results in a shift of the E point while preserving the overall curvature shape. The same cannot be said about the overall topological changes in the ED which have now become more complex since H has two different bonding partners. The TS is no longer a π-complex but closely resembles the E1 catastrophe structure and also as in the previous case no 3-membered ring was found. Here, an overall important observation is that the significant changes in the PES and ED, in

This journal is © The Royal Society of Chemistry [year]

Table 3 Local topological properties of the electron density $\rho(c)$ calculated at the bond critical points c along the IRC for the forming bond N2H3 and cleaving bond C1H3, values in bold are for curvature peak data. s reaction parameter, $\rho(c)$ electron density, $\nabla^2\rho(c)$ Laplacian, $H(c)$ total energy density, ε ellipticity calculated at the MP2/6-31G(d,p) level of theory

Numbering	Bond	Character	s (amu$^{1/2}$Bohr)	$\rho(c)$ (e/Bohr^3)	$\nabla^2\rho(c)$ (e/Bohr^5)	ε	$H(c)$ (Hartree/Bohr^3)
	C1H3	R	-3.3935	0.2916	-1.2087	0.0000	-0.3404
H3—C1≡N2 ⟶ C1≡N2—H3		TS	0.0000	0.2015	-0.3274	0.8648	-0.1741
		E1	0.0199	-	-	-	-
		M1	0.2999	-	-	-	-
		K1	0.7598	-	-	-	-
		M2	1.1398	-	-	-	-
		P	4.2527	-	-	-	-
	N2H3	R	-3.3935	-	-	-	-
		TS	0.0000	-	-	-	-
		E1	0.0199	0.2011	-0.3148	0.9183	-0.1724
		M1	0.2999	0.2038	-0.2577	1.1146	-0.1721
		K1	**0.7598**	**0.2386**	**-0.6623**	**0.4024**	**-0.2716**
		M2	1.1398	0.2650	-1.0479	0.1686	-0.3543
		P	4.2527	0.3384	-1.8678	0.0000	-0.5190

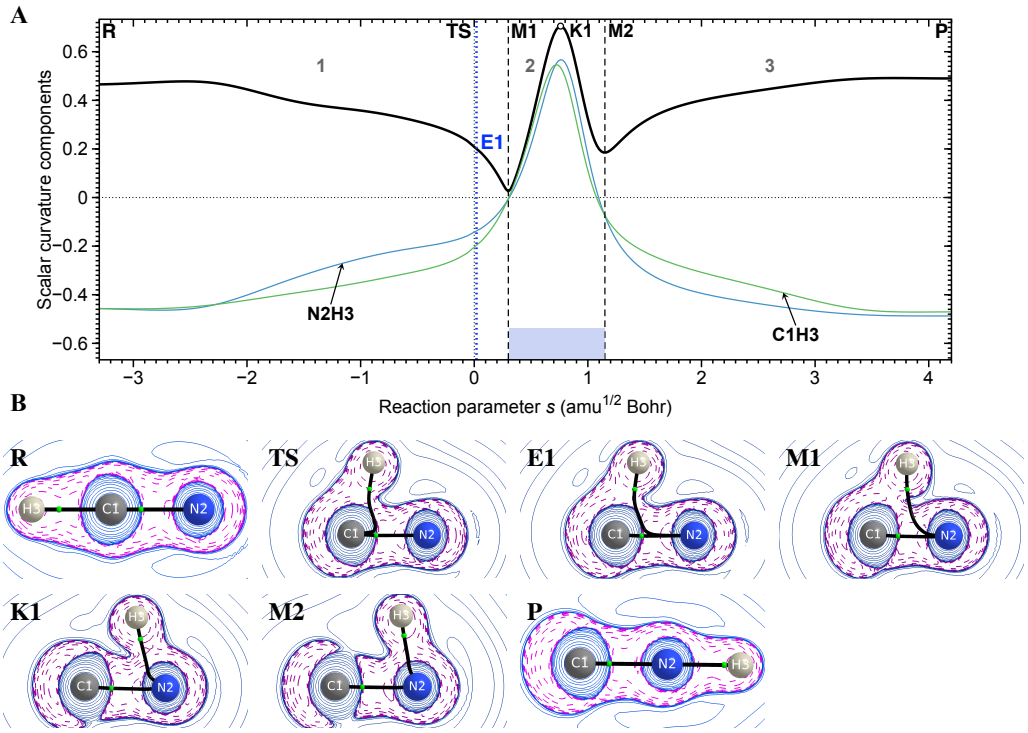

Fig. 5 R4 A) Scalar curvature as a function of the reaction parameter *s* (solid black line). The decomposition of scalar curvature into components is given in color. The borders of the reaction phases are indicated by vertical dashed lines at curvature points M1,M2,M3,etc. The TS at *s* = 0 amu$^{1/2}$ Bohr is also indicated by a vertical dashed line. R and P mark the first and last curvature points, corresponding to reactant and product respectively. K1,K2,etc. denote curvature peaks. E1,E2,etc. denote special points in electron density shown by blue vertical dashed lines. Values in grey 1,2,3,etc. indicate reaction phases and highlighted region in blue shows the chemical phases. B) Laplacian contour plots of selected curvature points R,TS,E1,M1,K1,M2,P, plotted in the molecular plane. The dashed (pink) contours denote regions of charge concentration where $\nabla^2\rho(\mathbf{r}) < 0$, and the solid (blue) contours denote regions of charge depletion where $\nabla^2\rho(\mathbf{r}) > 0$.

the simultaneous process of C1H3 bond cleavage and N2H3 bond formation, do not necessarily overlap on the reaction path but are accompanied by one another. The bond catastrophe in the ED at E1 occurs well in advance of curvature peak at K1, latter dictating the final cleavage of the existing bond and the establishing of the new bond.

3.4. R9: [3,3]-sigmatropic rearrangement of allyl acetate

This reaction has been studied in previous studies[62] including URVA[16], in connection with the gold-catalyzed counterpart (reaction **R10**, see ESI) to understand the mechanistic differences, particularly the influence of Au(I)-NHC catalysts[63,64] As revealed by curvature peaks, the rupture of the C10O4 bond takes place at K3 (-4.00 s units) and the formation of the new C16O5 bond at K5 (+3.79 s units) peaks (see Figure 6-A). From R through K3, the

Table 4 Local topological properties of the electron density $\rho(c)$ along the IRC calculated at the bond critical points c for the selected bonds C16O5,C1C16,C10O4, values in bold are for curvature peak data. s reaction parameter, $\rho(c)$ electron density, $\nabla^2\rho(c)$ Laplacian, $H(c)$ total energy density, ε ellipticity calculated at the B3LYP/6-31+G(d,p) level of theory

Numbering	Bond	Character	s (amu$^{1/2}$Bohr)	$\rho(c)$ (e/Bohr^3)	$\nabla^2\rho(c)$ (e/Bohr^5)	ε	$H(c)$ (Hartree/Bohr^3)
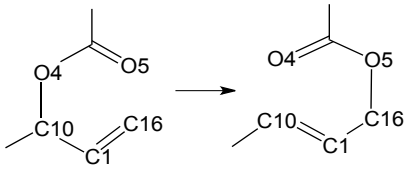	O4C10	R	-16.5259	0.2260	-0.3863	0.0147	-0.2897
		M1	-16.1438	0.2261	-0.3866	0.0145	-0.2897
		M2	-13.5044	0.2261	-0.3907	0.0135	-0.2891
		M3	-9.1552	0.2248	-0.3917	0.0167	-0.2845
		M4	-5.5260	0.2151	-0.3698	0.0209	-0.2554
		K3	**-3.9963**	**0.1902**	**-0.2633**	**0.0274**	**-0.1798**
		E1	-3.4264	0.1673	-0.1427	0.0328	-0.1243
		M5	-2.1366	0.1108	0.0627	0.0524	-0.0403
		TS	0.0000	0.0554	0.1218	0.1231	-0.0051
		K4	0.1571	0.0580	0.1214	0.1161	-0.0060
		M6	2.1367	0.0338	0.1129	0.2371	0.0005
		E2	3.3364	0.0281	0.1016	0.3064	0.0014
		K5	**3.7863**	**0.0263**	**0.0960**	**0.3363**	**0.0015**
		M7	5.0161	0.0220	0.0801	0.4463	0.0017
		M8	9.8151	0.0135	0.0470	1.6929	0.0014
		M9	17.9135	-	-	-	-
		P	19.3478	-	-	-	-
	C16O5	R	-16.5259	-	-	-	-
		M1	-16.1438	-	-	-	-
		M2	-13.5044	-	-	-	-
		M3	-9.1552	-	-	-	-
		M4	-5.5260	0.0179	0.0665	0.9268	0.0018
		K3	**-3.9963**	**0.0238**	**0.0891**	**0.5881**	**0.0019**
		E1	-3.4264	0.0262	0.0969	0.4913	0.0018
		M5	-2.1366	0.0325	0.1109	0.3203	0.0009
		TS	0.0000	0.0542	0.1232	0.1151	-0.0045
		K4	0.1571	0.0517	0.1230	0.1261	-0.0037
		M6	2.1367	0.1123	0.0630	0.0446	-0.0414
		E2	3.3364	0.1693	-0.1506	0.0362	-0.1286
		K5	**3.7863**	**0.1889**	**-0.2545**	**0.0348**	**-0.1768**
		M7	5.0161	0.2108	-0.3528	0.0293	-0.2434
		M8	9.8151	0.2243	-0.3872	0.0194	-0.2841
		M9	17.9135	0.2283	-0.3891	0.0222	-0.2964
		P	19.3478	0.2287	-0.3882	0.0238	-0.2978
	C1C16	R	-16.5259	0.3456	-1.0087	0.3638	-0.3874
		M1	-16.1438	0.3456	-1.0089	0.3638	-0.3875
		M2	-13.5044	0.3459	-1.0108	0.3637	-0.3881
		M3	-9.1552	0.3467	-1.0160	0.3629	-0.3895
		M4	-5.5260	0.3475	-1.0210	0.3616	-0.3912
		K3	**-3.9963**	**0.3471**	**-1.0196**	**0.3563**	**-0.3901**
		E1	-3.4264	0.3463	-1.0169	0.3495	-0.3883
		M5	-2.1366	0.3417	-0.9991	0.3193	-0.3784
		TS	0.0000	0.3203	-0.9059	0.2199	-0.3343
		K4	0.1571	0.3225	-0.9159	0.2289	-0.3388
		M6	2.1367	0.2855	-0.7466	0.1033	-0.2658
		E2	3.3364	0.2690	-0.6703	0.0578	-0.2351
		K5	**3.7863**	**0.2655**	**-0.6548**	**0.0475**	**-0.2287**
		M7	5.0161	0.2639	-0.6495	0.0386	-0.2253
		M8	9.8151	0.2637	-0.6525	0.0354	-0.2239
		M9	17.9135	0.2638	-0.6554	0.0305	-0.2234
		P	19.3478	0.2639	-0.6561	0.0340	-0.2236

This journal is © The Royal Society of Chemistry [year]

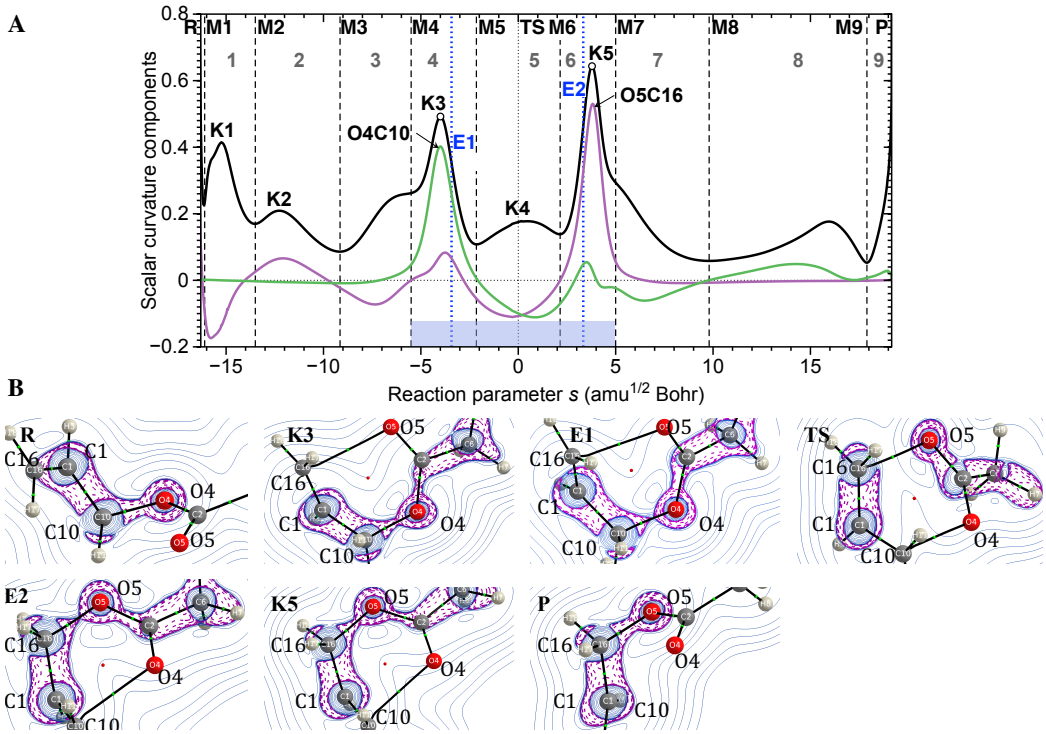

Fig. 6 R9 A) Scalar curvature as a function of the reaction parameter s (solid black line). The decomposition of scalar curvature into components is given in color. The borders of the reaction phases are indicated by vertical dashed lines at curvature points M1,M2,M3,etc. The TS at s = 0 amu$^{1/2}$ Bohr is also indicated by a vertical dashed line. R and P mark the first and last curvature points, corresponding to reactant and product respectively. K1,K2,etc. denote curvature peaks. E1,E2,etc. denote special points in electron density shown by blue vertical dashed lines. Values in grey 1,2,3,etc. indicate reaction phases and highlighted region in blue shows the chemical phases. B) Laplacian contour plots of selected curvature points R,E1,K3,TS,K5,E2,P plotted in the planes C1-O4-C10 for R-E1 and O5-C1-C16 for TS-P. The dashed (pink) contours denote regions of charge concentration where $\nabla^2\rho(\mathbf{r}) < 0$, and the solid (blue) contours denote regions of charge depletion where $\nabla^2\rho(\mathbf{r}) > 0$.

ED starts depleting between the C10O4 atomic basins (see Figure 6-B), as represented by the decreasing negative $\nabla^2\rho(c)$ and H(c) values at C10O4 (see Table 4). At E1 (-3.43 s units), located in the close vicinity of K3 peak, the overlapping VSCC is separated into their respective atomic basins, C10 and O4. As could be anticipated, afterwards this point, $\nabla^2\rho(c)$ is becoming positive, marking the transition of the C10O4 shared-shell interaction to that of a closed-shell interaction. Subsequently, the covalent character of the C4H10 bond is deteriorating as viewed in the decrease of negative H(c) values. It is interesting to notice that at E1 the supporting contribution of the O4C10 curvature component has already begun to decrease as well as the small supporting contribution from O5C16. Shortly after the TS at K4 peak, both O4C10 and C16O5 components are resisting further change and as discovered by URVA this indicates the possibility to break up the reaction into two steps with the use of a catalyst[16] which is demonstrated in the reaction **R10**. At E2 (+3.55 s units, see Figure 6-B), the formation of the C16O5 bond is initiated when VSCC overlap occurs leading to the ED accumulation between the C16O5 atomic basins and bond formation is represented by K5 peak. Both O5C16 and O4C10 components are supporting at this point yet the supporting contribution from latter starts to decline shortly after E1. When the ED starts to flow into the O5C16 region this component positively influences the curving of the reaction path. In contrast, the ED has substantially depleted from the O4C10 region at this point and the O4C10 component is affecting the curving of the reaction path to a lesser degree, or in other words it is suppressing further curving. In agreement with former results, the O4C10 bond cleavage is followed by E1, and E2 precedes the O5C16 bond formation.

3.5. Decomposition of $H(c)$ along the reaction path The energy density $H(\mathbf{r})$ is defined as:[39,65]

$$H(\mathbf{r}) = \mathbf{G}(\mathbf{r}) + \mathbf{V}(\mathbf{r}) \tag{1}$$

and its connection to the Laplacian $\nabla^2\rho(\mathbf{r})$ is given by the *Virial Theorem*:[20–22]

$$\frac{1}{4}\nabla^2\rho(\mathbf{r}) = 2G(\mathbf{r}) + \mathbf{V}(\mathbf{r}) \tag{2}$$

where $G(\mathbf{r})$ is the kinetic energy density (always positive) and $V(\mathbf{r})$ (always negative) is the potential energy density. The negative potential energy $V(\mathbf{r})$ corresponds to a stabilizing accumulation of density whereas the positive kinetic energy density $G(\mathbf{r})$ corresponds to a depletion of electron density.[39]. Therefore, the inspection of how $G(c)$ and $V(c)$ change along the reaction path and how these changes are connected with the changes observed in $\nabla^2\rho(c)$, in particular in bond formation/cleavage regions will lead to a deeper understanding of the PES-ED relationship. This

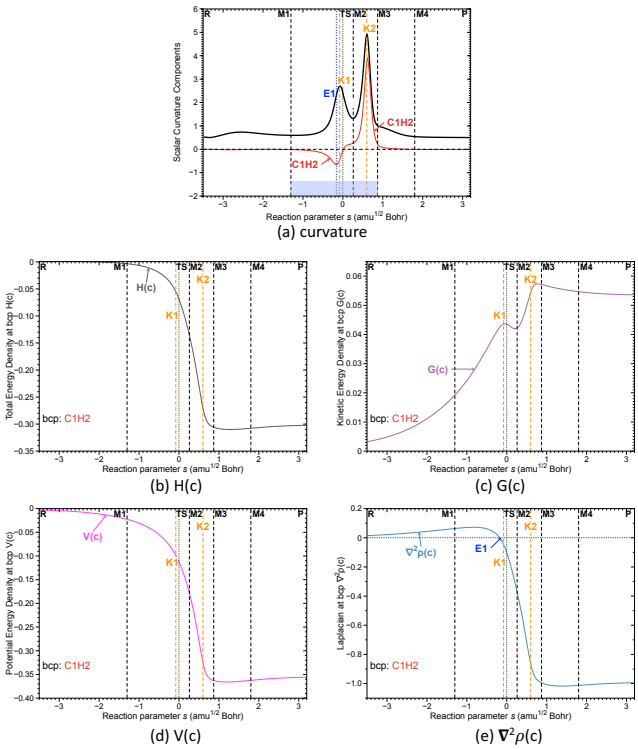

Fig. 7 Decomposition of $H(c)$ for the C1H2 bond along the reaction path along the reaction path for **R2**. The curvature peak positions, K1 and K2 are indicated by orange vertical dashed lines. The E point is indicated either by a blue vertical dashed line or marked in blue. The reaction path is calculated in s (amu$^{1/2}$Bohr) units. $H(c)$, $G(c)$ and $V(c)$ are in Hartree/Bohr^3 units. The Laplacian is given in e/Bohr^5 units. (a) Curvature (in black) and the curvature contribution of the bond forming component C1H2 (in red); (b) Total energy density $H(c)$ along the reaction path; (c) Kinetic energy density $G(c)$ along the reaction path; (d) Potential energy density $V(c)$ along the reaction path; (e) Laplacian $\nabla^2\rho(c)$ along the reaction path.

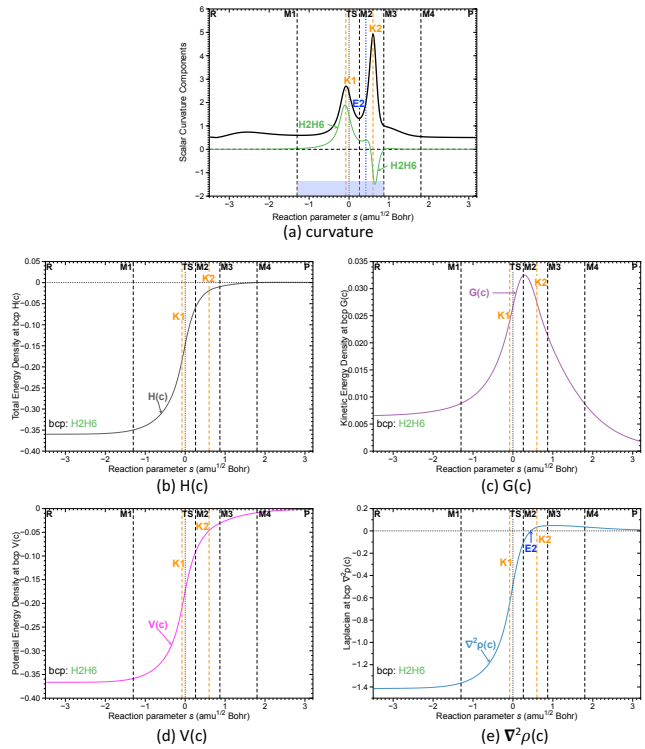

Fig. 8 Decomposition of $H(c)$ for the H2H6 bond along the reaction path along the reaction path for **R2**. The curvature peak positions, K1 and K2 are indicated by orange vertical dashed lines. The E point is indicated either by a blue vertical dashed line or marked in blue. The reaction path is calculated in s (amu$^{1/2}$Bohr) units. $H(c)$, $G(c)$ and $V(c)$ are in Hartree/Bohr^3 units. The Laplacian is given in e/Bohr^5 units. (a) Curvature (in black) and the curvature contribution of the bond cleavage component H2H6 (in green); (b) Total energy density $H(c)$ along the reaction path; (c) Kinetic energy density $G(c)$ along the reaction path; (d) Potential energy density $V(c)$ along the reaction path; (e) Laplacian $\nabla^2\rho(c)$ along the reaction path.

is discussed in the following for **R2** as an example. Figure 7 shows how $H(c)$, $G(c)$, $V(c)$ and $\nabla^2\rho(c)$ change for the C1H2 bond (bond to be formed) along the reaction path and Figure 8 shows the corresponding changes for the H2H6 bond (bond to be broken). For the C1H2 bond, we observed that $H(c)$ becomes negative close to curvature minimum M1 before the K1 peak, which implies that $V(\mathbf{r})$ becomes dominating onwards this point. $G(c)$ increases up to the curvature point K2, however the increase is not strong enough to outweigh $H(c)$. $\nabla^2\rho(c)$ starts out to be positive, slightly increasing until the E1 point is reached, where it changes sign from positive to negative (see Figure 7-e) indicating that electrons are confined to the bonding region. The link to the reaction path curvature is given by the fact that at the E1 point the C1H2 component of the reaction path curvature changes from the negative (i.e. resisting) to positive (i.e. supporting) as a consequence of electrons being more trapped in the C1H2 bond region, eventually leading to bond formation. In the H2H6 bond cleavage event (see Figure 8), after M1 $V(c)$ is decreasing and in contrast $G(c)$ is increasing reaching a maximum value around M2. After this point kinetic energy density becomes dominating as shown by the sign transition of $\nabla^2\rho(c)$ from negative to positive (E2 point, see Figure 8-e). The link to the reaction path curvature is given by the fact that after E2 the supporting contribution from the H2H6 component rapidly declines and as kinetic energy density has already reached a maximum in H2H6 region, it implies electrons are less likely to stay in that region or in other words H2H6 bond has been cleaved. In summary, this analysis shows that there is a direct connection between the interplay of $V(c)$ and $G(c)$ and the reaction path curvature.

4 Conclusions

In this work, we unravelled the relationship between the reaction path curvature peaks associated with bond formation/cleavage events and changes in the topology of the ED, vindicating the Hohenberg-Kohn theorem. For all reactions **R1** - **R10** investigated in this work the ED changes connected with a bond formation/cleavage process occurred in the vicinity of the corresponding curvature peak. As illustrated in this work, a combined URVA-QTAIM study provides a comprehensive view on bond formation/cleavage processes seen through the eyes of both the PES and ED. It also offers valuable guidelines where to search for significant ED changes associated with a bond formation/cleavage

This journal is © The Royal Society of Chemistry [year]

event. We could arrive at the following conclusions.

(1) Scanning the neighborhood of a curvature peak associated with a bond formation/cleavage event with QTAIM exposed the manifold of changes in the ED. These changes are reflected in the topology of Laplacian as beginning of VSCC overlap between respective atomic basins inducing the bond formation or conversely, the ceasing of the VSCC overlap, leading to a bond cleavage. Additionally, catastrophe points of the conflict and bifurcation type could be identified in the close vicinity of a curvature peak, where bond paths appear/disappear or bond and ring critical points coalesce. These significant changes in the ED along the reaction path connected with a bond formation/cleavage event always appeared close to a curvature peak. Thus, the location of the curvature peaks can serve as starting points for an ED analysis of bond formation/cleavage processes within the QTAIM framework. This replaces the cumbersome exercise of scanning the entire reaction path to monitor topological changes in order to determine the location bond formation/cleavage, as has been the approach of some previous studies.

(2) The locations of the reaction path curvature peaks denoting bond formation or bond cleavage events are concomitant to notable changes in the topology of the ED. For bond formation events significant ED changes occur before or at the curvature peak, and as a corollary, for bond cleavage events, the topological changes indicated by the disappearance of a bond path or ceasing of VSCC overlap between two atomic basins occur either at or shortly after the peak. We quantified the shift of the E points relative to the corresponding bond formation/cleavage curvature peak and results are included in ESI (see Table S7). The largest deviation in the E point is observed for **R7** bond formation which is shifted about 26% relative to the respective curvature peak. The other pericyclic reactions **R6** and **R8** show similar deviations except in **R9** which has a very slight deviation as low as 1-2% for both bond formation and cleavage events. The delay in bond formation in **R6**, **R7** and **R8** compared to **R9** can be explained by the electronegativity difference of the two bonding partners. In the latter, the ED is exchanged between the C and O atoms which is more efficient and leads to an early bond formation opposed to C-C bond formation in **R6**, **R7** and **R8**. For all the other reactions E point deviations up to 11% are observed which suggest these E points are in close proximity to the corresponding curvature peaks. This information can be used as a useful guide in an ED analysis, particularly to narrow down the region scanned around the curvature peak.

(3) Decomposition of $H(c)$ into kinetic and potential energy density contributions along the reaction path revealed that the relationship between PES and ED is mainly governed by the interplay of $V(c)$ and $G(c)$ where the latter reaches a maximum near Kn and Mn. As a consequence, significant changes in the ED occur close to a curvature peak.

(4) This combined URVA-QTAIM study leads us to further solidify the fact that the TS is mechanistically often not relevant in accordance with previous URVA studies.[12] We observed for all reactions studied in this work, with the exception of **R3** (see ESI) where TS/E/K points coincide because of symmetry, that the curvature peaks associated with bond formation/cleavage events are located before or after the TS. We also could not find any specific changes in the ED at the TS locations.

(5) A topological analysis going beyond the stationary points on the PES (R,TS,P) probing the nature of bonding at the reaction path curvature maxima and minima as well provides a comprehensive new understanding of bond formation/cleavage events.

5 Acknowledgement

This work was financially supported by National Science Foundation [CHE 1464906]. We thank SMU for providing computational resources.

References

1 K. Fukui, *Accounts Chem. Res.*, 1981, **14**, 363–368.
2 L. Komorowski, P. Ordon and M. Jędrzejewski, *Phys. Chem. Chem. Phys.*, 2016, **18**, 32658–32663.
3 S. Gutiérrez-Oliva, S. Díaz, A. Toro-Labbé, P. Lane, J. S. Murray and P. Politzer, Molecular Physics, 2014, pp. 349–354.
4 J. Martínez and A. Toro-Labbé, *J. Math. Chem.*, 2009, **45**, 911–927.
5 P. Jaque, A. Toro-Labbé, P. Politzer and P. Geerlings, *Chem. Phys. Lett.*, 2008, **456**, 135–140.
6 E. Kraka and D. Cremer, *Accounts Chem. Res.*, 2010, **43**, 591–601.
7 D. Cremer and E. Kraka, *Curr. Org. Chem.*, 2010, **14**, 1524–1560.
8 E. Kraka, *WIREs Comput. Mol. Sci.*, 2011, **1**, 531–556.
9 W. H. Miller, N. C. Handy and J. E. Adams, *J. Chem. Phys.*, 1980, **72**, 99–112.
10 W. Zou, T. Sexton, E. Kraka, M. Freindorf and D. Cremer, *J. Chem. Theory Comput.*, 2016, **12**, 650–663.
11 C. S. López, O. N. Faza, M. Freindorf, E. Kraka and D. Cremer, *J. Org. Chem.*, 2016, **81**, 404–414.
12 T. Sexton, E. Kraka and D. Cremer, *J. Phys. Chem. A*, 2016, **120**, 1097–1111.
13 M. Freindorf, T. Sexton, E. Kraka and D. Cremer, *Theor. Chem. Acc.*, 2013, **133**, 1423–1441.
14 E. Kraka, W. Zou, M. Freindorf and D. Cremer, *J. Chem. Theory Comput.*, 2012, **8**, 4931–4943.
15 E. Kraka, H. Joo and D. Cremer, *Mol. Phys.*, 2010, **108**, 19–20.
16 M. Freindorf, D. Cremer and E. Kraka, *Mol. Phys.*, 2017, **116**, 611–630.
17 M. Castiñeira Reis, C. S. López, E. Kraka, D. Cremer and O. N. Faza, *Inorga. Chem.*, 2016, **55**, 8636–8645.
18 M. Freindorf, Y. Tao, D. Sethio, D. Cremer and E. Kraka, *Mol. Phys.*, 2019, **117**, 117–1192.
19 P. Hohenberg and W. Kohn, *Phys. Rev.*, 1964, **136**, B864–B871.
20 R. F. Bader, *Atoms in Molecules: A Quantum Theory*, Clarendon Press, Oxford, U.K., 1990.
21 R. F. W. Bader, *Chem. Rev.*, 1991, **91**, 893–928.
22 R. F. W. Bader, *Acc. Chem. Res.*, 1985, **18**, 9–15.
23 R. F. W. Bader, *Monatshefte für Chemie*, 2005, **136**, 819–854.
24 C. F. Matta and R. J. Gillespie, *J. Chem. Educ.*, 2002, **79**,

1141–1152.
25 H. J. Bohórquez, R. J. Boyd and C. F. Matta, *J. Phys. Chem. A*, 2011, **115**, 12991–12997.
26 C. F. Matta and R. J. Boyd, *The Quantum Theory of Atoms in Molecules: From Solid State to DNA and Drug Design*, Wiley-VCH, Weinheim, Germany, 2007.
27 A. D. Becke and K. E. Edgecombe, *J. Chem. Phys.*, 1990, **92**, 5397–5403.
28 X. Krokidis, S. Noury and B. Silvi, *J. Phys. Chem. A*, 1997, **101**, 7277–7282.
29 A. I. Adjieufack, I. M. Ndassa, I. Patouossa, J. K. Mbadcam, V. S. Safont, M. Oliva and J. Andrés, *Phys. Chem. Chem. Phys.*, 2017, **19**, 18288–18302.
30 E. Zahedi, S. Shaabani and A. Shiroudi, *J. Phys. Chem. A*, 2017, **121**, 8504–8517.
31 M. F. Zalazar and N. M. Peruchena, *J. Mol. Model.*, 2011, **17**, 2501–2511.
32 D. Chakraborty, C. Cárdenas, E. Echegaray, A. Toro-Labbe and P. W. Ayers, *Chem. Phys. Lett.*, 2012, **539-540**, 168–171.
33 T. Berlin, *J. Chem. Phys.*, 1951, **19**, 208–213.
34 C. Sun, Y. Zeng, L. Meng and S. Zheng, *Chin. J. Chem. Phys.*, 2007, **21**, 123–130.
35 R. F. W. Bader, P. J. MacDougall and C. D. H. Lau, *J. Am. Chem. Soc.*, 1984, **106**, 1594–1605.
36 D. Cremer and E. Kraka, *Theoretical Models of Chemical Bonding. The Concept of the Chemical Bond*, Springer Verlag, Heidelberg, 1990, vol. 2, p. 453.
37 T. Lu and F. Chen, *J. Phys. Chem. A*, 2013, **117**, 3100–3108.
38 E. Espinosa, C. Lecomte and E. Molins, *Chem. Phys. Lett.*, 1999, **300**, 745–748.
39 D. Cremer and E. Kraka, *Croat. Chem. Acta*, 1984, **57**, 1259–1281.
40 Z. Konkoli, E. Kraka and D. Cremer, *J. Phys. Chem. A*, 1997, **101**, 1742–1757.
41 E. Kraka, A. Wu and D. Cremer, *J. Phys. Chem. A*, 2003, **107**, 9008–9021.
42 D. Cremer, A. Wu and E. Kraka, *Phys. Chem. Chem. Phys.*, 2001, **3**, 674–687.
43 H. Joo, E. Kraka, W. Quapp and D. Cremer, *Mol. Phys.*, 2007, **105**, 2697–2717.
44 E. Kraka, *Encyclopedia of Computational Chemistry*, John Wiley & Sons, New York, 1998, vol. 4, pp. 2437–2463.
45 T. M. Sexton, M. Freindorf, E. Kraka and D. Cremer, *J. Phys. Chem. A*, 2016, **120**, 8400–8418.
46 D. Cremer, *Wiley Interdisciplinary's: Computational Molecular Science*, John Wiley & Sons, New York, 2011, vol. 1, pp. 509–530.
47 D. Cremer, *Encyclopedia of Computational Chemistry*, John Wiley & Sons, Chichester, UK, 1998, vol. 3, p. 1706.
48 P. Hariharan and J. Pople, *Theor. Chim. Acta.*, 1973, **28**, 213–222.
49 F. Weigend and R. Ahlrichs, *Phys. Chem. Chem. Phys.*, 2005, **7**, 3297–3305.
50 D. Andrae, U. Haeussermann, M. Dolg, H. Stoll and H. Preuss, *Theor. Chim. Acta.*, 1990, **77**, 123–141.
51 A. Becke, *J. Chem. Phys.*, 1993, **98**, 5648–5652.
52 T. Clark, J. Chandrasekhar, G. W. Spitznagel and P. V. R. Schleyer, *J. Comput. Chem.*, 1983, **4**, 294–301.
53 R. Ditchfield, W. Hehre and J. Pople, *J. Chem. Phys.*, 1971, **54**, 724–728.
54 P. Schwerdtfeger, M. Dolg, W. Schwarz, G. Bowmaker and P. Boyd, *J. Chem. Phys.*, 1989, **91**, 1762–1774.
55 M. J. Frisch, G. W. Trucks, H. B. Schlegel, G. E. Scuseria, M. A. Robb, J. R. Cheeseman, G. Scalmani, V. Barone, G. A. Petersson, H. Nakatsuji, X. Li, M. Caricato, A. V. Marenich, J. Bloino, B. G. Janesko, R. Gomperts, B. Mennucci, H. P. Hratchian, J. V. Ortiz, A. F. Izmaylov, J. L. Sonnenberg, D. Williams-Young, F. Ding, F. Lipparini, F. Egidi, J. Goings, B. Peng, A. Petrone, T. Henderson, D. Ranasinghe, V. G. Zakrzewski, J. Gao, N. Rega, G. Zheng, W. Liang, M. Hada, M. Ehara, K. Toyota, R. Fukuda, J. Hasegawa, M. Ishida, T. Nakajima, Y. Honda, O. Kitao, H. Nakai, T. Vreven, K. Throssell, J. A. Montgomery, Jr., J. E. Peralta, F. Ogliaro, M. J. Bearpark, J. J. Heyd, E. N. Brothers, K. N. Kudin, V. N. Staroverov, T. A. Keith, R. Kobayashi, J. Normand, K. Raghavachari, A. P. Rendell, J. C. Burant, S. S. Iyengar, J. Tomasi, M. Cossi, J. M. Millam, M. Klene, C. Adamo, R. Cammi, J. W. Ochterski, R. L. Martin, K. Morokuma, O. Farkas, J. B. Foresman and D. J. Fox, *Gaussian 16*, 2016, (Gaussian, Inc., Wallingford CT, 2016).
56 T. A. Keith, 2017, AIMALL TK Gristmill Software, Overland Park, KS.
57 E. Kraka, W. Zou, M. Filatov, J. Gräfenstein, D. Izotov, J. Gauss, Y. He, A. Wu, Z. Konkoli, V. Polo, L. Olsson, Z. He and D. Cremer, *COLOGNE201919*, Dallas, Texas, 2019.
58 J. Jankunas, M. Sneha, R. N. Zare, F. Bouakline, S. C. Althorpe, D. Herraez-Aguilar and F. J. Aoiz, *Proc. Natl. Acad. of Sci.*, 2014, **111**, 15–20.
59 A. Michalak and T. Ziegler, *J. Phys. Chem. A*, 2001, **105**, 4333–4343.
60 M. P. Mitoraj, M. Parafiniuk, M. Srebro, M. Handzlik, A. Buczek and A. Michalak, *J. Mol. Model.*, 2011, **17**, 2337–2352.
61 L. Deng and T. Ziegler, *Int. J. Quantum Chem.*, 1994, **52**, 731–765.
62 C. Gourlaouen, N. Marion, S. P. Nolan and F. Maseras, *Org. Lett.*, 2009, **11**, 81–84.
63 S. Díez-González, N. Marion and S. P. Nolan, *Chem. Rev.*, 2009, **109**, 3612–3676.
64 N. Marion, R. Gealageas and S. P. Nolan, *Org. Lett.*, 2007, **9**, 2653–2656.
65 D. Cremer and E. Kraka, *Angew. Chem. Int. Ed.*, 1984, **23**, 627–628.

This journal is © The Royal Society of Chemistry [year]
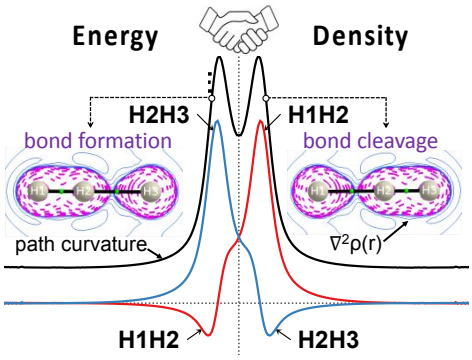
The first combined quantum chemical energy-electron density description of bond breaking/forming events using URVA and QTAIM.